Characterization of Forced Flame Response of Swirl-Stabilized Turbulent Lean-Premixed Flames in a Gas Turbine Combustor

Kyu Tae Kim

Jong Guen Lee[1]
e-mail: jxl145@psu.edu

Hyung Ju Lee

Bryan D. Quay

Domenic A. Santavicca

Department of Mechanical and Nuclear Engineering,
The Pennsylvania State University,
University Park, PA 16802

Flame transfer function measurements of turbulent premixed flames are made in a model lean-premixed, swirl-stabilized, gas turbine combustor. OH, CH*, and CO_2* chemiluminescence emissions are measured to determine heat release oscillation from a whole flame, and the two-microphone technique is used to measure inlet velocity fluctuation. 2D CH* chemiluminescence imaging is used to characterize the flame shape: the flame length ($L_{CH^* max}$) and flame angle (α). Using H_2-natural gas composite fuels, X_{H2} = 0.00–0.60, a very short flame is obtained and hydrogen enrichment of natural gas is found to have a significant impact on the flame structure and flame attachment points. For a pure natural gas flame, the flames exhibit a "V" structure, whereas H_2-enriched natural gas flames have an "M" structure. Results show that the gain of M flames is much smaller than that of V flames. Similar to results of analytic and experimental investigations on the flame transfer function of laminar premixed flames, it shows that the dynamics of a turbulent premixed flame is governed by three relevant parameters: the Strouhal number ($St = L_{CH^* max}/L_{conv}$), the flame length ($L_{CH^* max}$), and the flame angle ($\alpha$). Two flames with the same flame shape exhibit very similar forced responses, regardless of their inlet flow conditions. This is significant because the forced flame response of a highly turbulent, practical gas turbine combustor can be quantitatively generalized using the nondimensional parameters, which collapse all relevant input conditions into the flame shape and the Strouhal number.* [DOI: 10.1115/1.3204532]

1 Introduction

The term "combustion instability" generally refers to the sustained high amplitude pressure fluctuations in a combustion chamber, resulting from the coupling between the system acoustics and the unsteady heat release. It is by nature a self-excited oscillation, involving complicated physical phenomena such as unsteady combustion, acoustic fluctuations, heat transfer, and the vorticity field. A large number of studies using experimental, theoretical, and numerical simulation approaches have been performed to investigate instability mechanisms, controlling parameters, and active or passive control methodologies to suppress the instability intensity level to acceptable ranges. Ultimately, to accurately predict instability characteristics at the development stage, a complete understanding of the nature of combustion instabilities will be required and sophisticated theoretical models must be developed [1,2].

The development of a theoretical model capable of predicting the formation of combustion-driven pressure oscillations is contingent on the physical understanding of the response of a flame to periodic disturbances. Heat release perturbations occur for several reasons, such as inlet velocity fluctuations, equivalence ratio fluctuations, and perturbations of thermodynamic properties. For turbulent, totally premixed flames, the direct influence of equivalence ratio, pressure, temperature, and density variations on the heat release rate perturbations is negligible [3]. For this type of flame, the inlet velocity fluctuation is dominant, and it governs the flame dynamics. To quantitatively describe the response of a flame to upstream perturbations, the flame transfer function (*FTF*) is introduced, defined as the normalized ratio of heat release and velocity fluctuations

$$FTF(f,A) = \frac{Q'(f)/\bar{Q}}{V'(f)/\bar{V}} \tag{1}$$

where $\bar{Q}$ is the time-averaged heat release rate, $\bar{V}$ is the mean velocity of the mixture in the mixing section, $Q'(f)$ and $V'(f)$ are their corresponding amplitudes at the forcing frequency f, and A is the magnitude of $V'(f)/\bar{V}$. The flame transfer function can be obtained by experimental [4–7], theoretical [8–10], and numerical [11–13] methods. The flame transfer function is mathematically formulated and used in the thermoacoustic network modeling as a source term to predict self-induced combustion instability [14,15].

Transfer functions of laminar premixed flames subjected to inlet velocity perturbations have been investigated in detail [16,17]. Schuller et al. [16] showed that the dynamics of laminar premixed flames are governed by two relevant parameters: a reduced frequency $\omega_* = (\omega R)/(S_L \cos \alpha)$ and the flame angle (α). Fleifil et al. [17] examined the response of laminar premixed flame to flow oscillations using an analytical model, and they described how the flame transfer function depends primarily on the flame Strouhal number, defined as $\omega R/S_L$. Lieuwen [18] reported that the flame transfer function of premixed flames depends strongly on three parameters: a Strouhal number $St = \omega L_f/u_0$, the ratio of the flame length to width $\beta = L_f/R$, and the flame shape (i.e., conical and inverted wedge). Later, Preetham and Lieuwen [9] compared the response of laminar and turbulent premixed flames to harmonic velocity oscillations. They showed that the qualitative dynamics of the flames remain similar with significant quantitative differences. Several other studies have focused on the nonlinear response of turbulent premixed flames, since an understanding of a

[1]Corresponding author.

Manuscript received March 21, 2009; final manuscript received March 30, 2009; published online January 19, 2010. Review conducted by Dilip R. Ballal.

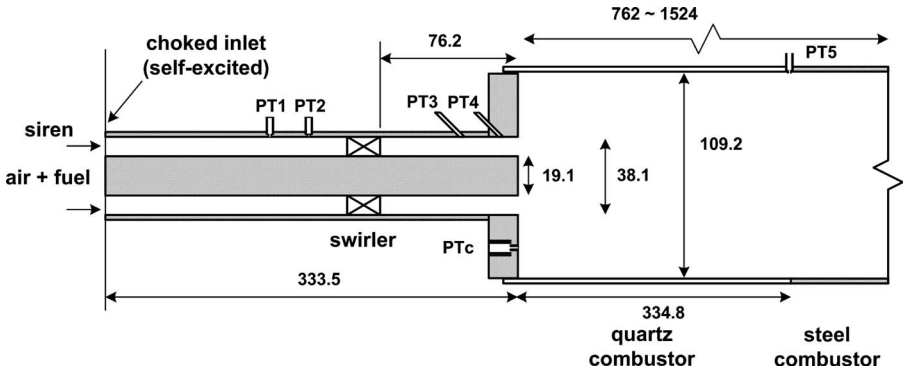

Fig. 1 Schematic of a swirl-stabilized, lean-premixed, gas turbine combustor. Dimensions in millimeters.

combustor's nonlinear dynamics is critical to the prediction of the limit-cycle oscillation amplitude [4–6]. Systematic parametric studies designed to determine the relevant parameters governing the forced response of swirl-stabilized, turbulent premixed flames are, however, rare. In this study, we focus on the dependence of the response of a turbulent premixed flame subjected to inlet velocity perturbations upon the flame shape. The nondimensional parameters governing the forced response of turbulent premixed flames in a lean-premixed, swirl-stabilized, gas turbine combustor will also be discussed. The results will then be compared with data on laminar premixed flames.

2 Experimental Methods

All measurements are performed in a lean-premixed, variable-length, gas turbine combustor facility, shown in Fig. 1. This facility consists of an air inlet section, a siren, a mixing section, an optically-accessible quartz combustor section, a steel combustor section, and an exhaust section. The air can be heated to a maximum temperature of 400°C by a 30 kW electric heater. Two high-temperature globe valves are used to control the bypass flow rate, i.e., the inlet velocity fluctuation amplitudes. A siren-type modulation device is used to provide acoustic modulations. The siren is driven by a variable-speed dc motor, which permits changing of the forcing frequency (100–400 Hz). The mixing section is 0.333 m long and has an annular cross section that is defined by a 19.1 mm o.d. centerbody and a 38.1 mm i.d. mixing tube. The centerbody is centered in the mixing tube, and it is positioned such that its downstream end is flush with the combustor dump plane. A 30 deg flat-vane axial swirler is mounted in the mixing tube at 76.2 mm upstream of the combustor dump plane. Fuel (natural gas+H_2) is injected and mixed with air at upstream of the choked inlet in order to eliminate equivalence ratio fluctuations.

High-frequency response, water-cooled, piezoelectric pressure transducers (PCB 112A04) are used to measure pressure perturbations in the mixing (denoted by PT1–PT4 in Fig. 1) and the combustor (PTc and PT5) sections. The pressure signals are conditioned by amplifiers, digitized by an analog-to-digital converter, and stored in a microcomputer memory for processing at a sampling rate of 8192 Hz. A total of 16,384 data points are taken during each test. Two pressure transducers located at 12.7 mm (PT4) and 50.8 mm (PT3) upstream of the combustor dump plane are used to estimate the inlet velocity fluctuations using the two-microphone method [19,20]. To calibrate the two-microphone method, direct measurements of velocity fluctuations are performed under cold flow conditions with a hot wire anemometer (TSI 1210-20). Three photomultiplier tubes (PMT, Hamamatsu model H7732-10) are used to measure the global OH^* (307 ± 5 nm), CH^* (432 ± 5 nm), and CO_2^* (365 ± 5 nm) chemiluminescence emission intensities from the whole flame. An ICCD camera (Princeton Instruments model 576G) with a CH^* band pass filter centered at 430 nm (10 nm full width at half maxium) is used to record the flame images. Because CH^* chemiluminescence images are line-of-sight integrated images, a three-point Abel deconvolution scheme is used to extract two-dimensional information from the line-of-sight images.

All tests are performed at a mean pressure of 1 atm and at mean equivalence ratios ranging from 0.55 to 0.70. Mean velocity at the nozzle is varied from 60 to 100 m/s and the inlet temperature is kept constant at 200°C, giving a Reynolds number of approximately 33,000–54,000. Forcing frequency is varied from 100 Hz to 400 Hz. The range of forcing frequency is determined based on the two-microphone method calibration results. It is found that the uncertainty of the two-microphone method increases when the forcing frequency is lower than 100 Hz (a low-frequency limit) and greater than 450 Hz (a high-frequency limit). The neglect of wave attenuation between the microphones leads to a low-frequency limit for the application of the two-microphone method [20]. On the other hand, the high-frequency limit is determined by finite difference error and error due to uncertainty of the effective separation distance between the microphones [19]. Also, the frequency range of 100–400 Hz includes self-induced instability frequencies observed in the lean-premixed gas turbine combustor, shown in Fig. 1. To achieve a broad range of flame structures, H_2-blended natural gas fuels with $X_{H2}=0.00-0.60$ were utilized.

3 Results and Discussion

3.1 Effect of X_{H2} on Stable Flame Shapes. An overall understanding of the flame structure is gained from time-averaged CH^* chemiluminescence images, shown in Fig. 2. Figure 2 presents the dependence of the spatial distribution of the flame's heat release on H_2 mole fraction (X_{H2}) and equivalence ratio. In these deconvoluted images, only the upper half is shown because the reconstructed images are axisymmetric. The direction of flow is from left to right. With increasing X_{H2} (from 0.00 to 0.60) or equivalence ratio (from 0.55 to 0.70) at a fixed inlet velocity (60 m/s), the flame length decreases because of the increased flame propagation speed. The flame extends into the corner recirculation zone as well as the inner shear layer at an equivalence ratio of 0.55 with $X_{H2}=0.00$. Line-of-sight integrated (background-corrected) flame images for $\Phi=0.60$ ($T_{in}=200°C$; $V_{mean}=60$ m/s; premixed; and $X_{H2}=0.00$, 0.15, 0.30, 0.45, and 0.60), which corresponds to the second column in Fig. 2, are shown in Fig. 3. It can be observed that at $X_{H2}=0.30-0.60$, the flame is stabilized on the rapid expansion, i.e., at the combustor dump plane, as well as on the centerbody. The flame geometry changes from a simple V flame to an M (enveloped) flame with increasing H_2 mole fraction. This could be related to the increased flame propagation speed, since the same phenomenon has been observed in pure natural gas flames at the high equivalence ratio of $\Phi=0.70$. H_2-blended natural gas flames can be sustained in the

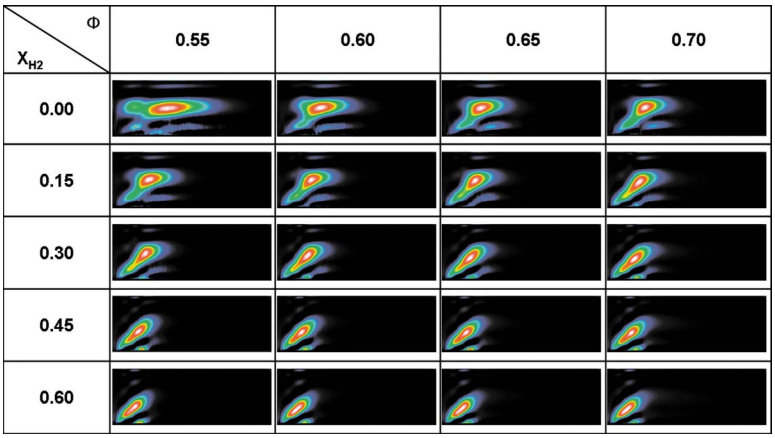

Fig. 2 Deconvoluted stable flame images (CH^* chemiluminescence). Operating conditions: T_{in}=200°C; V_{mean}=60 m/s; Φ=0.55, 0.60, 0.65, 0.70, and premixed; and X_{H2}=0.00, 0.15, 0.30, 0.45, and 0.60.

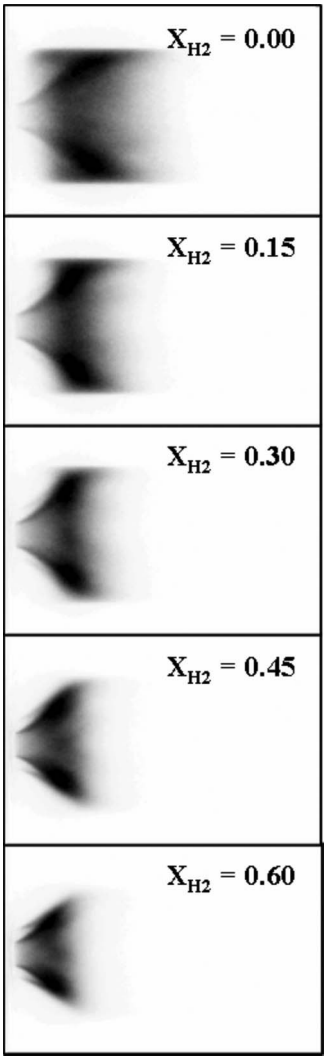

Fig. 3 Line-of-sight integrated flame images for X_{H2}=0.00, 0.15, 0.30, 0.45, and 0.60 from top to bottom. Operating conditions: T_{in}=200°C, V_{mean}=60 m/s, and Φ=0.60.

outer shear layer, i.e., in the high strain rate region, since the flame's extinction strain rate is enhanced. Studies of laminar premixed flames have reported that V flames are less stable than M flames because M flames produce weak flame surface fluctuations when they interact with flow disturbances [16,21]. The influence of these flame geometries on the forced response of swirl-stabilized, turbulent premixed flames will be discussed in Sec. 3.3. To quantitatively describe the flame shape, the distance between the edge of the centerbody and the maximum CH^* chemiluminescence intensity point ($L_{CH^* max}$), and the flame angle (α) between $L_{CH^* max}$ and the flow direction are defined from the deconvoluted flame images, shown in Fig. 2. $L_{CH^* max}$ represents the flame length. The dependence of the flame length $L_{CH^* max}$ upon the H_2 mole fraction for V_{mean}=90 m/s is shown in Fig. 4. It can be observed from Figs. 2 and 4 that the flame length is independent of the equivalence ratio at the H_2 mole fraction of X_{H2}=0.60. This result implies that when X_{H2} is greater than 0.60, varying the equivalence ratio does not affect changes in the convection time scale.

The coordinates of maximum CH^* chemiluminescence intensity locations and flame angle (α) versus the flame length $L_{CH^* max}$ of

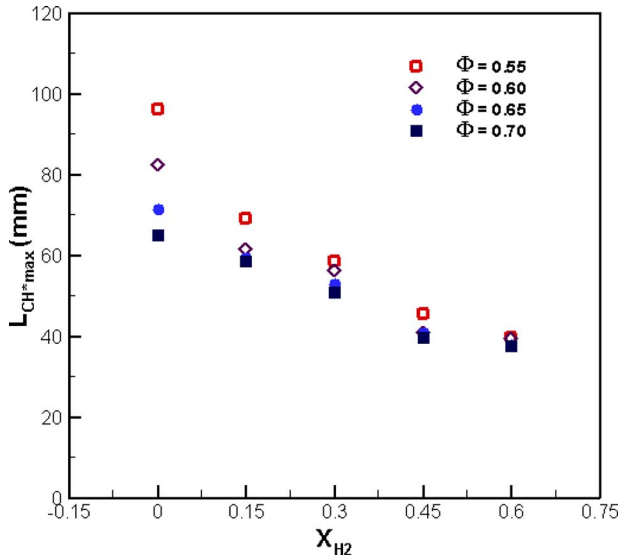

Fig. 4 Dependence of the flame length ($L_{CH^* max}$) upon H_2 mole fraction for V_{mean}=90 m/s

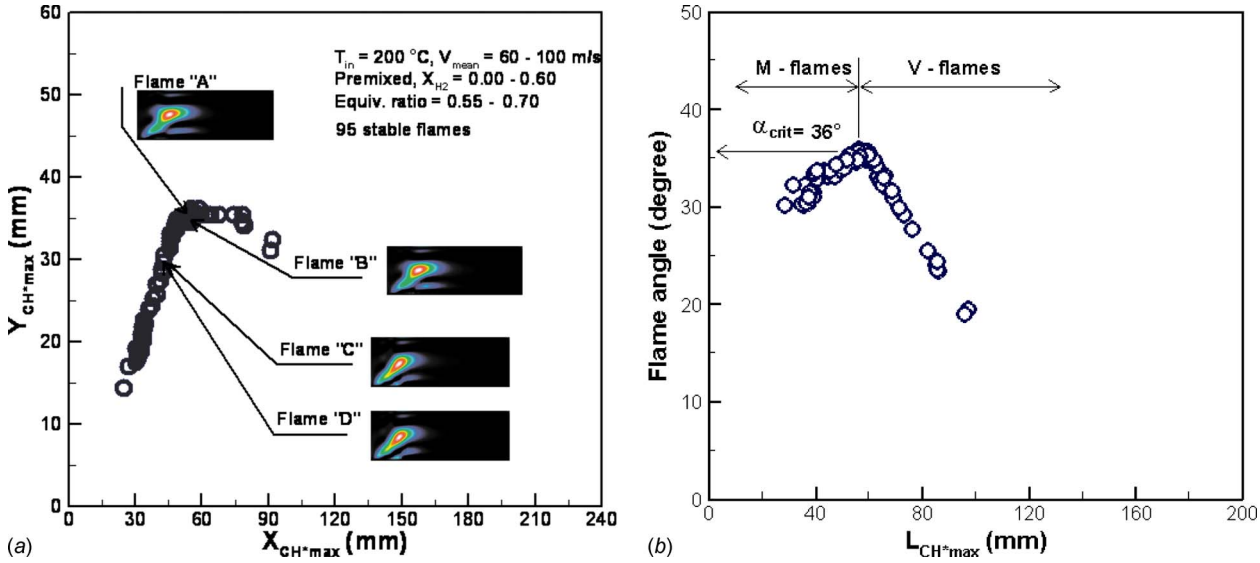

Fig. 5 Coordinates of maximum CH* chemiluminescence intensity locations and the flame angle (α) versus the flame length ($L_{CH^* max}$)

95 stable flames are shown in Fig. 5. The plots show that the maximum CH* chemiluminescence intensity locations can be characterized by a well-defined curve; $L_{CH^* max}$ varies along this curve over a range of input conditions. A similar observation was made by Figura et al. [22]. Figure 5 also shows that the flame angle α increases up to $\alpha_{crit} \sim 36$ deg, and then decreases as $L_{CH^* max}$ decreases. The critical flame angle α_{crit} corresponds to the demarcation point where V-flame geometries are changed to M flames as the flame length decreases. Therefore, the flame length $L_{CH^* max}$ and the flame angle α are necessary parameters to define the flame shape. These two parameters, $L_{CH^* max}$ and α, will be used to analyze the forced response of turbulent premixed flames in Sec. 3.3.

Table 1 Input parameters of four different flames

	T_{in} (°C)	V_{mean} (m/s)	ϕ	% H_2	T_{ad} (K)	Q_{in} (kW)	$L_{CH^* max}$ (mm)	α (deg)
A	200	60	0.65	0	1681	67.91	65.3	33
B	200	70	0.70	0	1767	84.90	63.5	33
C	200	60	0.70	15	1772	72.77	55.7	35
D	200	80	0.60	30	1609	84.21	55.9	35

3.2 Influence of Flame Shape on Forced Flame Response. Four flames were chosen as examples, to compare heat release responses. Flames "A" and "B" represent typical V flames and "C" and "D" represent typical M flames. Input conditions and deconvoluted flame images are presented in Table 1 and Fig. 5, respectively. Flames A and B have different input parameters, such as inlet velocity, equivalence ratio, adiabatic flame temperature, and input power, but they have a similar flame structure, i.e., $L_{CH^* max}$ and α. Figure 6 shows the gain of the flame transfer function of flames A and B as a function of the magnitude of inlet velocity fluctuation at forcing frequencies of f=100 and 250 Hz. The gain of the two different flames is almost identical at the two forcing frequencies. The results shown in Fig. 6 indicate that flames A and B show saturation phenomena at the same forcing

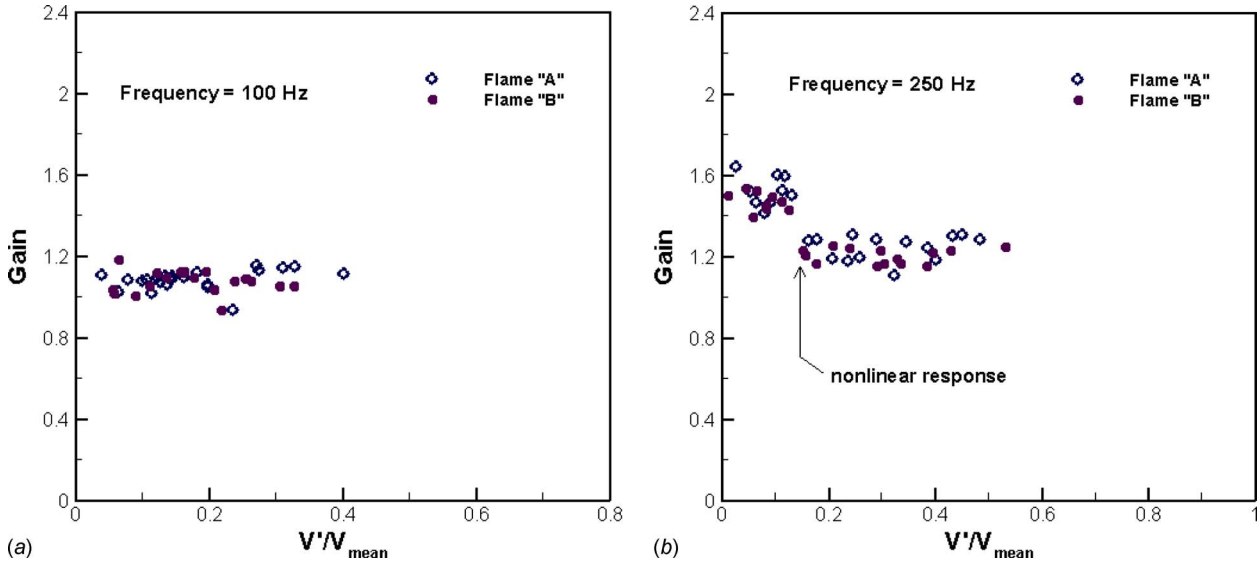

Fig. 6 Comparison of gain of flames A and B: f=100 and 250 Hz

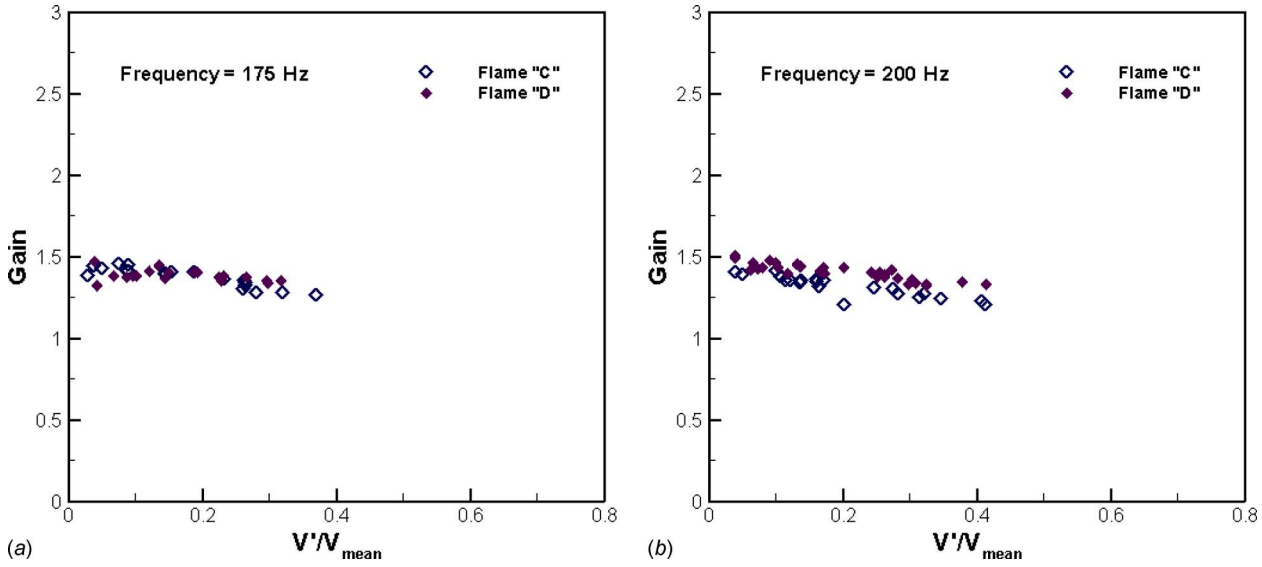

Fig. 7 Comparison of gain of flames C and D: f=175 and 200 Hz

amplitude, $V'/V_{\text{mean}} \sim 0.13$ (f=250 Hz). Figure 7 shows the gain of *FTF* of flames C and D, typical M flames, at forcing frequencies of 175 Hz and 200 Hz. Figure 7 clearly shows that the dynamic responses of flames C and D are also very similar. In particular, the forced response of these M flames remains in the linear regime at a forcing frequency of f=200 Hz and inlet velocity fluctuation magnitude of up to $V'/V_{\text{mean}} \sim 0.40$. At this point, coherent large-scale structures are developed. This suggests that the M flames are less influenced by the interaction with the vortex-ring structures, and therefore, the forced response is still in the linear regime. Phase-synchronized flame imaging is necessary to interpret this particular behavior of M flames. These results suggest that flame shape is one of important parameters governing the flame transfer functions of swirl-stabilized turbulent premixed flames.

3.3 Flame Transfer Function. Figure 8 shows the flame transfer function (*FTF*) defined by Eq. (1) for a constant forcing amplitude (V'/V_{mean}=10%). Other operating conditions are the same, except for the H_2 mole fraction, X_{H2}=0% and 15%. H_2-enrichment affects the flame length substantially, while the adiabatic temperatures (T_{ad}=1591 and 1596 K for X_{H2}=0.00 and 0.15, respectively) and input powers (Q_{in}=62.99 and 63.06 kW for X_{H2}=0.00 and 0.15, respectively) remain similar. As reported by recent studies [4,16,23], the global flame response can be described as a low-pass filter, in that the gain decreases as the frequency increases. These results also show that with increasing X_{H2}, the maximum gain of *FTF* decreases by 43% and the phase decreases at a given forcing frequency, indicating that the gain depends strongly on the flame length. As shown in the Fig. 8, the gain can be empirically fitted by a second-order model given by

$$n(\omega) = \left| \frac{K}{1 + i2\xi(\omega/\omega_c) - (\omega/\omega_c)^2} \right| \tag{2}$$

where ω_c corresponds to the angular frequency where gain of *FTF* reaches its maximum value and ξ is the damping coefficient,

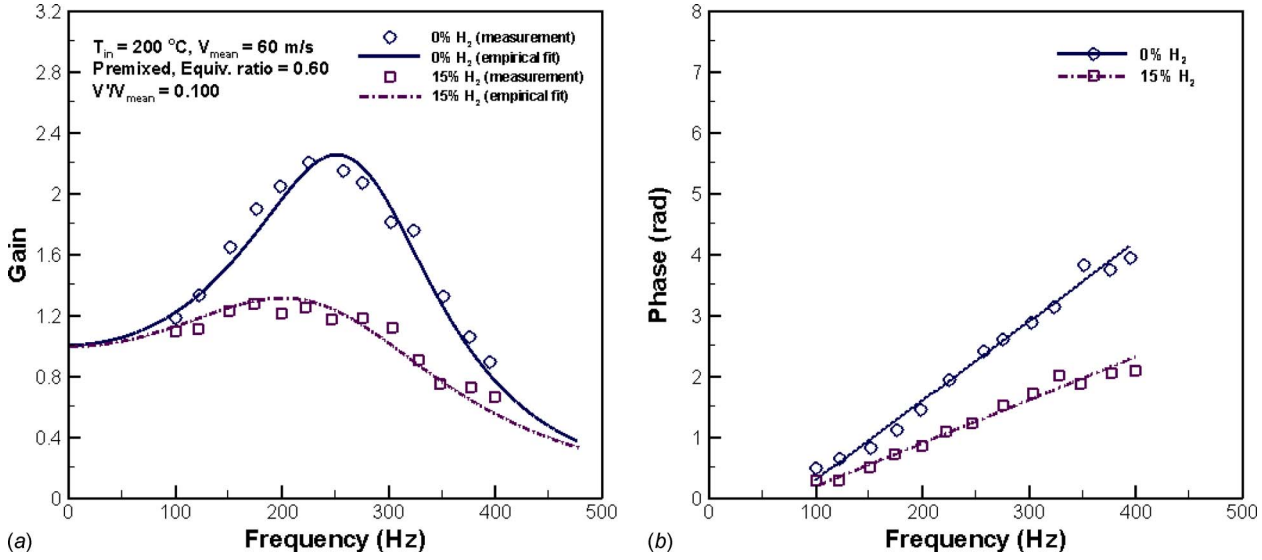

Fig. 8 Gain and phase difference of *FTF* versus forcing frequency at V'/V_{mean}=0.100. Operating conditions: T_{in}=200°C; V_{mean}=60 m/s; Φ=0.60 and premixed; and X_{H2}=0.00 and 0.15.

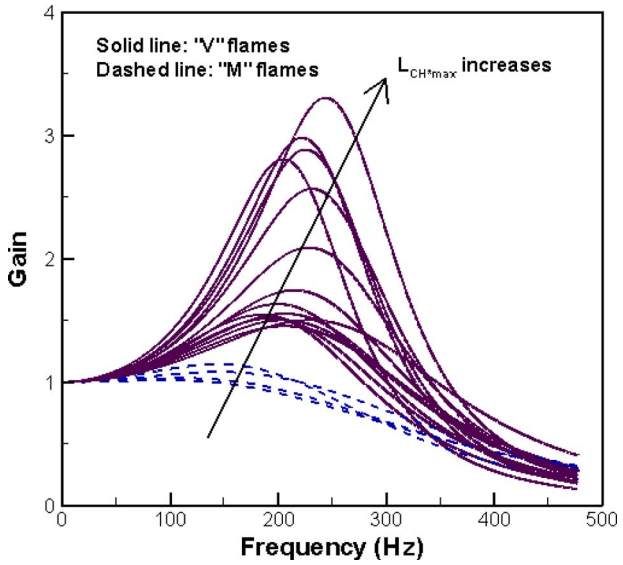

Fig. 9 Empirical fits (second-order oscillator model) of gain of *FTF* and maximum values of gain versus $L_{CH^* max}$. Operating conditions: $T_{in}=200\,^{\circ}C$; $V_{mean}=60$, 70, and 80 m/s; $\Phi=0.55$, 0.60, 0.65, 0.70, and premixed; and $X_{H2}=0.00$, 0.15, and 0.30.

which determines the highest value of gain at $\omega=\omega_c$. The phase can be approximated by Eq. (3)

$$\Delta\varphi = \tau\omega \tag{3}$$

where τ is the constant time delay. The parameters ξ, ω_c, and τ, obtained from the empirical fits, represent the dynamic characteristics of the global flame response to inlet velocity fluctuation.

Figure 9 shows empirical fits of the gain of *FTF* at a fixed forcing amplitude $V'/V_{mean}=10\%$ for various operating conditions ($X_{H2}=0.00$, 0.15, and 0.30; $T_{in}=200\,^{\circ}C$; $V_{mean}=60-80$ m/s; and $\Phi=0.55-0.70$). At the investigated operating conditions, the forced flame response is linear below the level of inlet perturbation of $V'/V_{mean}=10\%$. As the flame length gets shorter, the flame shape changes from V-to M-shaped flames. For the V flames, the gain is greatest over the frequency of 150–250 Hz and the flame acts as an amplifier. In the case of M flames, however, the overshoot behavior is not observed. It is interesting to note that the self-excited combustion instabilities in the combustor occur in the same frequency range of 150–250 Hz [24]. At high forcing frequencies $f>300$ Hz, the gain of *FTF* asymptotically approaches zero. Low-frequency flow perturbations significantly affect the global evolution of the flame surface area, i.e., the flame heat release rate. On the other hand, high-frequency velocity perturbations have a limited effect on the flame surface fluctuations [25]. The flame surface area does not vary under high-frequency modulation because of counteracting effect of bulges and cusps [26].

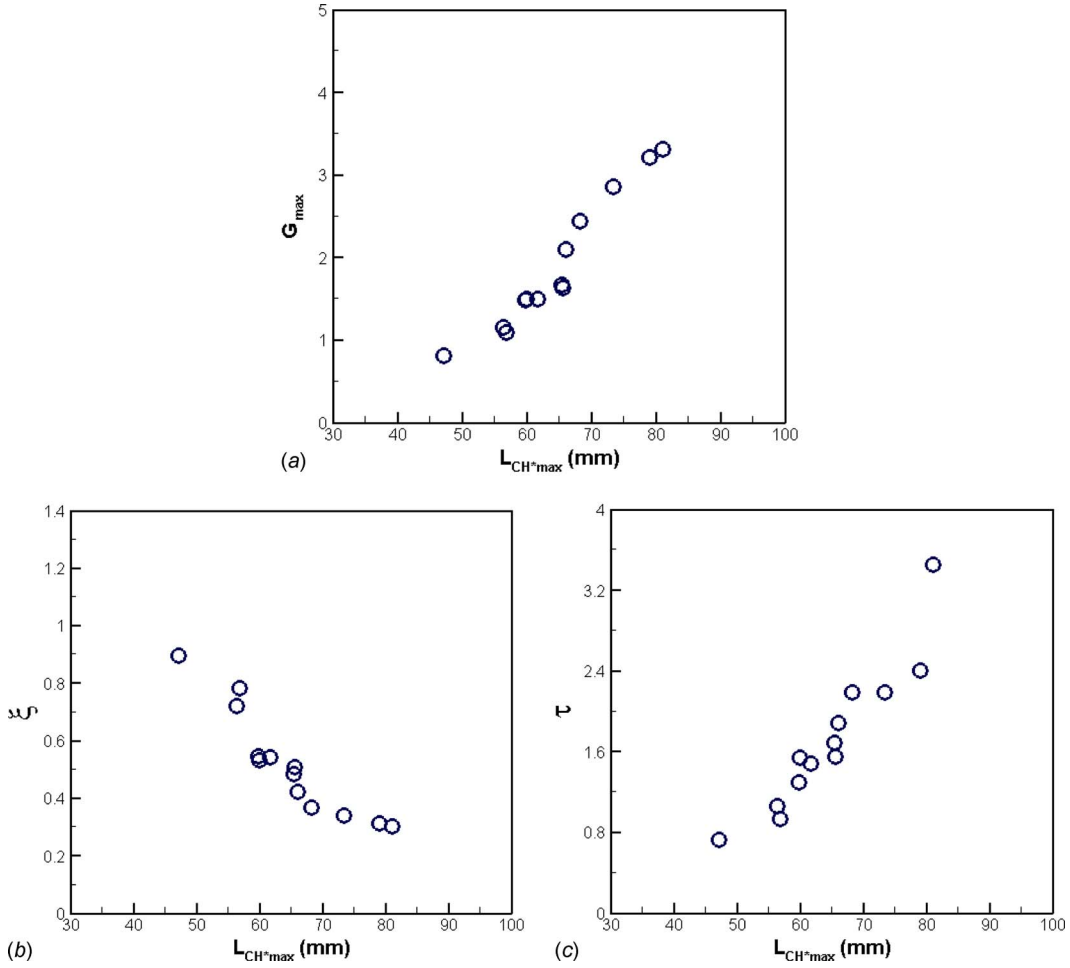

Fig. 10 Dependence of (*a*) maximum gain, (*b*) damping coefficient (ξ), and (*c*) convection time delay (τ) upon the flame length ($L_{CH^* max}$). Operating conditions: $T_{in}=200\,^{\circ}C$; $V_{mean}=60$, 70, and 80 m/s; $\Phi=0.55$, 0.60, 0.65, 0.70, and premixed; and $X_{H2}=0.00$, 0.15, and 0.30.

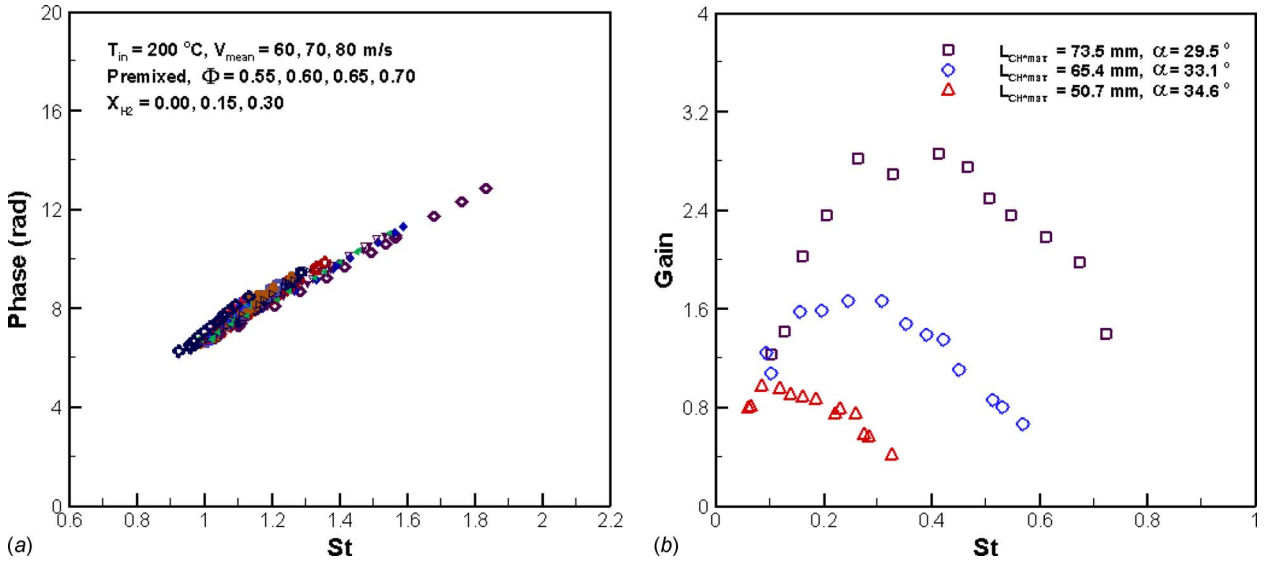

Fig. 11 Dependence of phase difference and gain of *FTF* on Strouhal number (St). Operating conditions: T_{in}=200°C; V_{mean}=60, 70, and 80 m/s; Φ=0.55, 0.60, 0.65, 0.70, and premixed; and X_{H2}=0.00, 0.15, and 0.30.

Figure 10 shows plots of maximum gain (G_{max}), damping coefficient (ξ), and convection time delay (τ), as a function of the flame length ($L_{CH^* max}$) at each operating condition. These results suggest that the flame dynamics are governed by the flame length as well as the perturbation frequency. The maximum gain of the *FTF* monotonically decreases with decreasing the flame length $L_{CH^* max}$, and this is true for both V and M flames. Figure 10(*b*) indicates that the decrease in maximum gain with respect to the decrease in the flame length is associated with the increased damping. The convection time delay τ is proportional to $L_{CH^* max}$, as shown in Fig. 10(*c*). This is mainly because the convection time for disturbances to reach the flame increases with increasing the flame length.

3.4 Controlling Parameters Governing *FTF* of Turbulent Premixed Flames. In Fig. 11, the gain and phase of *FTF* are plotted against the nondimensional parameter, the Strouhal number (St). The definition of St is presented in Eq. (4); it is calculated from the phase of *FTF* at each operating condition

$$\mathrm{St} = \frac{f \cdot L_{CH^* max}}{V_{conv}} = \frac{L_{CH^* max}}{L_{conv}} = \frac{\tau_{conv}}{T_{acoustic}} \quad (4)$$

The Strouhal number (St) represents the ratio of the flame length and the convective wavelength, or equivalently, the ratio of convective time to the acoustic forcing period. It is evident that the phase of *FTF* is well-characterized by the Strouhal number. When the flame angle changes significantly, the phase starts to deviate from the trend. On the other hand, the gain of *FTF* is a strong function of the flame shape as well as the Strouhal number. The gain decreases with increasing the flame angle (α). These results are reminiscent of the results from analytic and experimental studies about laminar premixed flames [9,16]. In an analytic study of V-flame transfer functions, Schuller et al. [16] reports that the smaller the flame angle, the larger and the higher the overshoot. They also show that phase difference is not significantly influenced by the flame angle α compared with the gain of *FTF*. Buchner et al. [27] reports that the dynamics of pulsated premixed axial jet flames are governed by the Strouhal number ($\mathrm{St} = f^* x_{OH^* max}/U$) only, but they do not take the flame structure into account. The results shown in Fig. 11 strongly suggest that the dynamic response of turbulent, swirl-stabilized, premixed flames is determined by three relevant parameters: the Strouhal number ($\mathrm{St} = L_{CH^* max}/L_{conv}$), the flame length ($L_{CH^* max}$), and the flame angle ($\alpha$). This also implies that to control the dynamics of turbulent premixed flames for the purpose of suppressing self-induced instabilities, either the Strouhal number or the flame shape should be modified.

4 Conclusions

A parametric study on the forced response of swirl-stabilized, turbulent premixed flames subjected to acoustic perturbations is performed. It is found that a simple V-flame geometry is modified to an M geometry when the flame propagation speed increases. The enveloped M flames have unique characteristics that allow them to damp flow perturbations, as compared with V flames. This suggests that natural gas flames with high H_2 mole fractions could be more stable in terms of combustion dynamics, but they could couple with the high-frequency acoustic eigenmodes of a system. The present results also show that the dynamics of swirl-stabilized, turbulent premixed flames are characterized by three relevant parameters: the Strouhal number ($\mathrm{St} = L_{CH^* max}/L_{conv}$), the flame length ($L_{CH^* max}$), and the flame angle ($\alpha$), thus extending previous experimental and analytical results from laminar to turbulent premixed flames. It would be interesting to assess these three parameters for other burner geometries. This is left for future studies. In this study, $L_{CH^* max}$ is used to represent the flame length (a single point), assuming that the ratio of the flame length to the acoustic wavelength is negligibly small. In practice, the flame has a distributed region of heat release, and therefore, the influence of the heat release distribution upon the response of the flame to forced and self-excited oscillations should be elucidated. There are currently no other experimental data on the controlling parameters of turbulent premixed flames in the literature. A systematic investigation of forced flame response measurements in a practical, lean-premixed, swirl-stabilized, gas turbine combustor could be incorporated into an analytic model and would enable the development of theoretical models for the control and suppression of self-sustained combustion instabilities.

References

[1] Lee, J. G., and Santavicca, D. A., 2003, "Experimental Diagnostics for the Study of Combustion Instabilities in Lean Premixed Combustors," J. Propul. Power, **19**(5), pp. 735–750.

[2] Candel, S., 2002, "Combustion Dynamics and Control: Progress and Challenges," Proc. Combust. Inst., **29**, pp. 1–28.

[3] Polifke, W., and Lawn, C., 2007, "On the Low-Frequency Limit of Flame Transfer Functions," Combust. Flame, **151**, pp. 437–451.

[4] Balachandran, R., Ayoola, B. O., Kaminski, C. F., Dowling, A. P., and Mastorakos, E., 2005, "Experimental Investigation of the Nonlinear Response of Turbulent Premixed Flames to Imposed Inlet Velocity Oscillations," Combust. Flame, **143**, pp. 37–55.
[5] Bellows, B. D., Neumeier, Y., and Lieuwen, T., 2006, "Forced Response of a Swirling, Premixed Flame to Flow Disturbances," J. Propul. Power, **22**, pp. 1075–1084.
[6] Kulsheimer, C., and Buchner, H., 2002, "Combustion Dynamics of Turbulent Swirling Flames," Combust. Flame, **131**, pp. 70–84.
[7] Lieuwen, T., and Neumeier, Y., 2002, "Nonlinear Pressure-Heat Release Transfer Function Measurements in a Premixed Combustor," Proc. Combust. Inst., **29**, pp. 99–105.
[8] You, D., Huang, Y., and Yang, V., 2005, "A Generalized Model of Acoustic Response of Turbulent Premixed Flame and Its Application to Gas-Turbine Combustion Instability Analysis," Combust. Sci. Technol., **177**, pp. 1109–1150.
[9] Preetham, S. H., and Lieuwen, T., 2007, "Response of Turbulent Premixed Flames to Harmonic Acoustic Forcing," Proc. Combust. Inst., **31**, pp. 1427–1434.
[10] Hirsch, C., Fanaca, D., Reddy, P., Polifke, W., and Sattelmayer, T., 2005, "Influence of the Swirler Design on the Flame Transfer Function of Premixed Flames," ASME Paper No. GT2005-68195.
[11] Armitage, C. A., Balachandran, R., Mastorakos, E., and Cant, R. S., 2006, "Investigation of the Nonlinear Response of Turbulent Premixed Flames to Imposed Inlet Velocity Oscillations," Combust. Flame, **146**, pp. 419–436.
[12] Sengissen, A. X., Van Kampen, J. F., Huls, R. A., Stoffels, G. G. M., Kok, J. B. W., and Poinsot, T. J., 2007, "LES and Experimental Studies of Cold and Reacting Flow in a Swirled Partially Premixed Burner With and Without Fuel Modulation," Combust. Flame, **150**, pp. 40–53.
[13] Gentemann, A., Hirsch, C., Kunze, K., Kiesewetter, F., Sattelmayer, T., and Polifke, W., 2004, "Validation of Flame Transfer Function Reconstruction for Perfectly Premixed Swirl Flames," ASME Paper No. GT2004-53776.
[14] Poinsot, T. J., and Veynante, D. P., 2005, *Theoretical and Numerical Combustion*, 2nd ed., Edwards, Ann Arbor, MI.
[15] Polifke, W., Poncet, A., Paschereit, C. O., and Dobbeling, K., 2001, "Reconstruction of Acoustic Transfer Matrices by Instationary Computational Fluid Dynamics," J. Sound Vib., **245**, pp. 483–510.
[16] Schuller, T., Durox, D., and Candel, S., 2003, "A Unified Model for the Prediction of Laminar Flame Transfer Functions: Comparisons Between Conical and V-Flame Dynamics," Combust. Flame, **134**, pp. 21–34.
[17] Fleifil, M., Annaswamy, A. M., Ghoneim, Z. A., and Ghoniem, A. F., 1996, "Response of a Laminar Premixed Flame to Flow Oscillations: A Kinematic Model and Thermoacoustic Instability Results," Combust. Flame, **106**, pp. 487–510.
[18] Lieuwen, T., 2005, "Nonlinear Kinematic Response of Premixed Flames to Harmonic Velocity Disturbances," Proc. Combust. Inst., **30**, pp. 1725–1732.
[19] Waser, M. P., and Crocker, M. J., 1984, "Introduction to the Two-Microphone Cross-Spectral Method of Determining Sound Intensity," Noise Control Eng. J., **22**, pp. 76–85.
[20] Abom, M., and Boden, H., 1988, "Error Analysis of Two-Microphone Measurements in Ducts With Flow," J. Acoust. Soc. Am., **83**, pp. 2429–2438.
[21] Schuller, T., Durox, D., and Candel, S., 2003, "Self-Induced Combustion Oscillations of Laminar Premixed Flames Stabilized on Annular Burners," Combust. Flame, **135**, pp. 525–537.
[22] Figura, L., Lee, J. G., Quay, B. D., and Santavicca, D. A., 2007, "The Effects of Fuel Composition on Flame Structure and Combustion Dynamics in a Lean Premixed Combustor," ASME Paper No. GT2007-27298.
[23] Kim, D., Lee, J. G., Quay, B. D., and Santavicca, D. A., 2008, "Effect of Flame Structure on the Flame Transfer Function in a Premixed Gas Turbine Combustor," ASME Paper No. GT2008-51014.
[24] Kim, K. T., Lee, H. J., Lee, J. G., Quay, B., and Santavicca, D., "Flame Transfer Function Measurement and Instability Frequency Prediction Using a Thermoacoustic Model," ASME Paper No. GT2009-60026.
[25] Huang, Y., and Yang, V., 2005, "Effect of Swirl on Combustion Dynamics in a Lean-Premixed Swirl-Stabilized Combustor," Proc. Combust. Inst., **30**, pp. 1775–1782.
[26] Ducruix, S., Durox, D., and Candel, S., 2000, "Theoretical and Experimental Determination of the Transfer Function of a Laminar Premixed Flame," Proc. Combust. Inst., **28**, pp. 765–773.
[27] Buchner, H., Hirsch, C., and Leuckel, W., 1993, "Experimental Investigation on the Dynamics of Pulsated Premixed Axial Jet Flames," Combust. Sci. Technol., **94**, pp. 219–228.